Electrochemical methodology for determination of imidazolium ionic liquids (solids at room temperature) properties: influence of the temperature†

M. P. Stracke,[a] M. V. Migliorini,[a] E. Lissner,[a] H. S. Schrekker,[a] D. Back,[b] E. S. Lang,[b] J. Dupont*[a] and R. S. Gonçalves*[a]

Received (in Gainesville, FL, USA) 17th July 2008, Accepted 29th August 2008
First published as an Advance Article on the web 14th October 2008
DOI: 10.1039/b812258j

A set of six imidazolium ionic liquids (**1a–b**, **2a–c**, **3**), that were solids at room temperature, were characterized by electrical impedance spectroscopy to obtain information about their polarization resistance (R_p), conductivity (σ) and charge transfer activation energy (E_a). These experiments were performed at different temperatures in a glass micro-cell, equipped with three platinum electrodes. The observed conductivities were due to charge transfer processes of molecular oxygen at the electrode surface and mass transfer processes within the IL matrix. Higher temperatures resulted for all ionic liquids in increased conductivities. X-Ray diffraction of the ionic liquids **2a–c** suggested that a higher degree of supramolecular two-dimensional organization, higher density, is related to an easier oxygen-electrode approximation, lower E_a. Two distinct temperatures ranges were observed. The larger conductivity increases in the higher temperature range were explained by melting (ILs **1–2**) and fluxional behavior/reorientation phenomena of the ionic liquids and are due to enhanced oxygen diffusion (IL **3**). In general, the understanding of imidazolium ionic liquid electrochemical properties could facilitate the development of new applications.

1. Introduction

The discovery of air- and water-stable imidazolium room-temperature ionic liquids (RTILs) by the suitable choice of the anion initiated intensive research efforts towards their application.[1] Further attractive physical and chemical properties of the imidazolium RTILs include,[2–6] a negligible vapor pressure; low inflammability; thermal stability; liquidity over a wide temperature range; easy recycling; and being a good solvent for a wide variety of organic and inorganic chemical compounds. Besides, imidazolium RTILs are "designable" as structural modifications in both the cation (especially the 1 and 3 positions of the imidazolium ring) and anion permit the tuning of properties such as, *e.g.*, miscibility with water and organic solvents,[7] melting point and viscosity.[3] This adaptability is also responsible for the easy preparation of task-specific imidazolium ionic liquids, ionic liquids that contain a specific functionality covalently incorporated in either the cation or anion.[8–11] As a result, applications of imidazolium RTILs are numerous and found in the fields of, for instance, extraction and separation processes,[4,12,13] synthetic chemistry,[4,6] catalysis (organometallic,[5,6,14,15] transition-metal nanoparticle,[14–19] bio[20]), and materials science.[4,21]

Another important imidazolium RTIL research area is in the field of electrochemistry, which is due to their chemical and electrochemical stability, wide electrochemical windows, and high electrical conductivities and ionic mobilities.[3–6,22–24] Electrochemical applications of imidazolium RTILs as electrolytes are found in, *e.g.*, fuel cells,[25] electrodeposition,[26] capacitors,[27–29] solar cells,[30,31] batteries[32] and water electrolysis for hydrogen generation.[33] However, the use of imidazolium RTILs could suffer from sealing problems due to leakage issues. Possible alternatives are, *e.g.*, imidazolium RTIL polymer homologues such as gel[34] or solid[35] polyelectrolytes, and imidazolium RTILs confined in silica-derived networks (ionogels)[36] and polymers.[27] Without doubt, the direct application of imidazolium ionic liquids (ILs), that are solids at room temperature, instead of imidazolium RTILs, would be another attractive option. As a consequence, we were interested in the electrochemical properties of imidazolium ILs (solids at room temperature). In general, understanding the physicochemical properties of ILs is of great importance to provide information about their application scope.[37,38] Herein, we report the results obtained with the imidazolium ILs **1–3**, presented in Fig. 1, which can be divided in two classes: (1) hydrophilic ILs **1a–b** and **3**, and (2) hydrophobic ILs **2a–c**. Electrical impedance spectroscopy (EIS), a non-destructive technique, was used to determine their temperature dependent polarization resistance (R_p), conductivity (σ) and charge transfer activation energy (E_a).

[a] *Laboratory of Electrochemistry, Laboratory of Molecular Catalysis and Laboratory of Technological Processes and Catalysis, Institute of Chemistry, Universidade Federal do Rio Grande do Sul, Av. Bento Gonçalves 9500, P.O. Box 15003, CEP: 91501-970 Porto Alegre-RS, Brazil. E-mail: dupont@iq.ufrgs.br; E-mail: reinaldo@iq.ufrgs.br; Fax: +55-51-3308-7304; Fax: +55-51-3308-7304; Tel: +55-51-3308-6321; Tel: +55-51-3308-7236*
[b] *Departamento de Química, Laboratório de Materiais Inorgânicos, Universidade Federal de Santa Maria, CEP: 97105-900 Santa Maria-RS, Brazil*

† Electronic supplementary information (ESI) available: Experimental section. CCDC 607218 (**2a**: room temperature), 607812 (**2b**: room temperature) and 671958 (**2c**: 100 K). For ESI and crystallographic data in CIF or other electronic format see DOI: 10.1039/b812258j

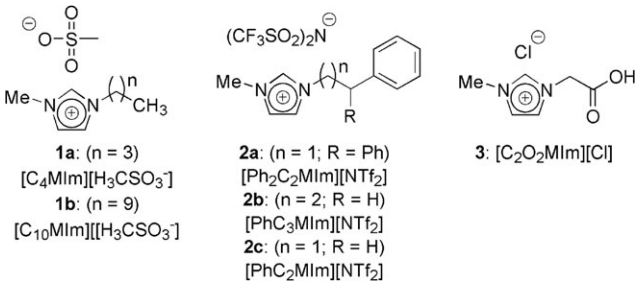

Fig. 1 Imidazolium ionic liquids (solid at room temperature) applied in this work.

2. Experimental

2.1 Imidazolium ionic liquids

The de-aerated imidazolium ILs **1a–b**,[39,40] **2a–c**[41–44] and **3**[45] were prepared according to known procedures, and the NMR spectral data were in agreement with the literature data. Recrystallizations were performed to obtain high purity ILs as white solids at room temperature.

2.2 Electrical impedance spectroscopy

The device used to perform the electrical impedance measurements of the room-temperature ionic solids consisted of a home-made glass micro-cell (Fig. 2) with a free area of 0.65 cm^2, equipped with three platinum wire electrodes. This micro-cell was inserted in a three-way round-bottom flask allowing the control of the gas atmosphere and humidity. The working electrode was located at the center of the micro-cell, the counter electrode was placed at the full length of the inner wall, and the reference electrode was located in between the working and counter electrodes. A computer-controlled potentiostat Autolab PGSTAT 30 was connected to the ionic solid in the glass-cell by the corresponding electrodes, and the temperature were kept under control. The electrical impedance spectra were measured over the frequency sweep range from 50 kHz to 5 Hz and the amplitude of the applied sine wave voltage was 10 mV. The experimental data were corrected by the software, taking into consideration the influence of connecting cables and other parasite capacitances, to obtain the polarization resistance (R_p) of the samples. The R_P values were obtained from the intercepts of the electrode impedance arc on the real impedance axis and were used to calculate the corresponding conductivities (σ).

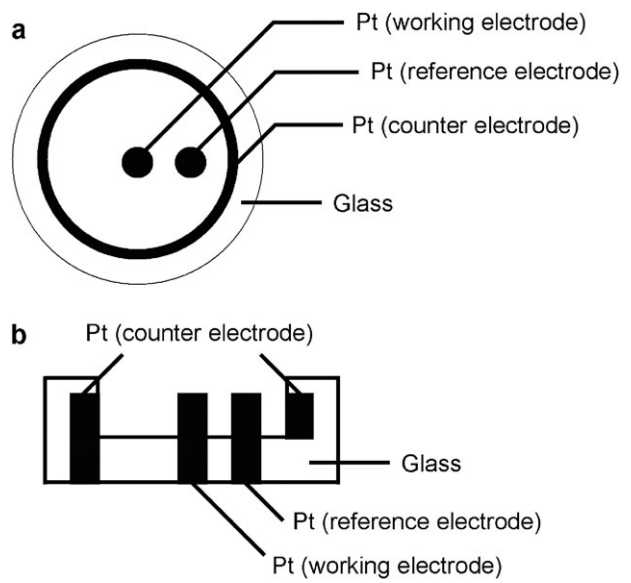

Fig. 2 Illustration of the home-made glass micro-cell: (a) top view; (b) section.

2.3 Differential scanning calorimetry

The melting points of the ILs **1a–b** and **2a–c** were determined using a TA Instruments DSC 2010 differential scanning calorimeter, equipped with a manual cooling unit. The DSC instrument was calibrated using an indium primary standard. An average sample weight of 7–12 mg was sealed in an aluminium pan in a nitrogen-filled glove box. The DSC measurements were carried out under a nitrogen atmosphere. The melting points (T_m, determined at the maximum of the endothermic peaks) were determined on heating in the second heating run.

2.4 X-Ray diffraction studies

Crystallographic data were collected at room temperature and/or −100 °C on a Bruker Kappa Apex II CCD diffractometer using Mo-Kα radiation (λ = 0,71073 Å). The experimental set-up did not allow full rotations. Hence, the data sets are of lower coverage. Crystal structures were refined with full-matrix least squares on F^2 using all data (SHELXTL crystal structure solution software). Non-hydrogen atoms were refined anisotropically. Hydrogen atoms were fixed on geometrically ideal positions during the refinement. The free refinement of hydrogen atom parameters gave low data/parameter ratios and led to high correlations. Relevant crystallographic data, and collection and refinement details, are compiled in Table S5 of ESI.† The structures presented in Fig. 6 were obtained from the original X-ray data using the DIAMOND software (version 2.1c, Crystal Impact GbR, http://www.crystalimpact.com/diamond/).

3. Results and discussion

3.1 Impedance spectrum analysis

A home-made glass micro-cell (Fig. 2), equipped with three platinum wire electrodes, was used for the electrical impedance spectroscopy measurements of the imidazolium ILs **1–3** (Fig. 1). Furthermore, the partial oxygen pressure of the gas atmosphere was kept constant. The Nyquist plots of IL [PhC_3MIm][NTf_2] **2b** at different temperatures are presented in Fig. 3(a). As for most of the ILs **1–3**, electrical impedance spectroscopy measurements with **2b** afforded partial semi-circles. An equivalent circuit is proposed taking into account that there exists a semicircle corresponding to one time constant that represents an electrochemical circuit with two resistances and one parallel combination of phase constant (CPE, Fig. S1, ESI†). In contrast, complete semicircles were observed with IL [C_2O_2MIm][Cl] **3** at higher temperatures (Fig. 3(b)). Performance of these electrical impedance spectroscopy measurements under vacuum resulted in confuse and irreproducible

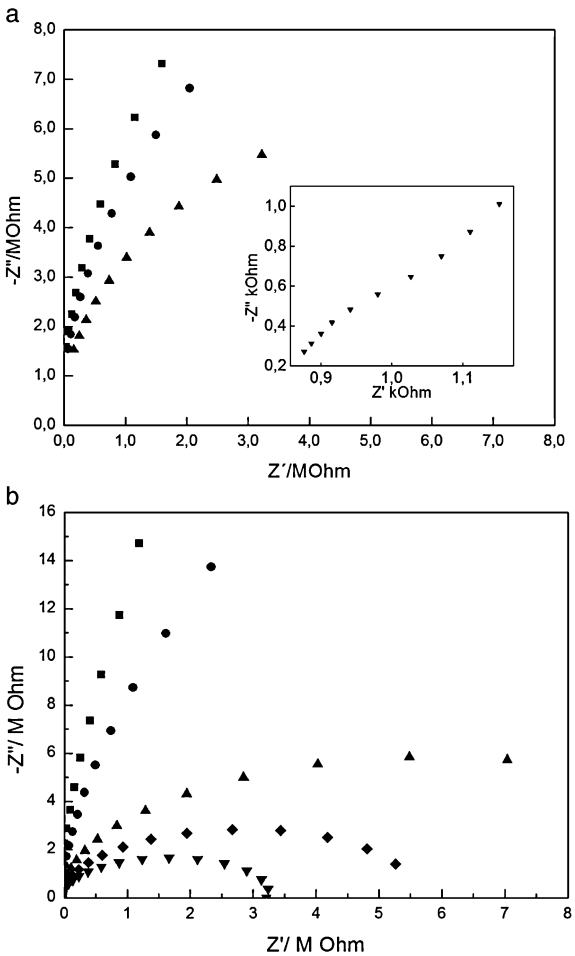

Fig. 3 (a) Nyquist diagram of $[PhC_3MIm][NTf_2]$ **2b** at 19 °C (■), 26 °C (●), 42 °C (▲) and 60 °C (window); (b) Nyquist diagram of $[C_2O_2MIm][Cl]$ **3** at 5 °C (■), 17 °C (●), 31 °C (▲), 34 °C (◆) and 42 °C (▼).

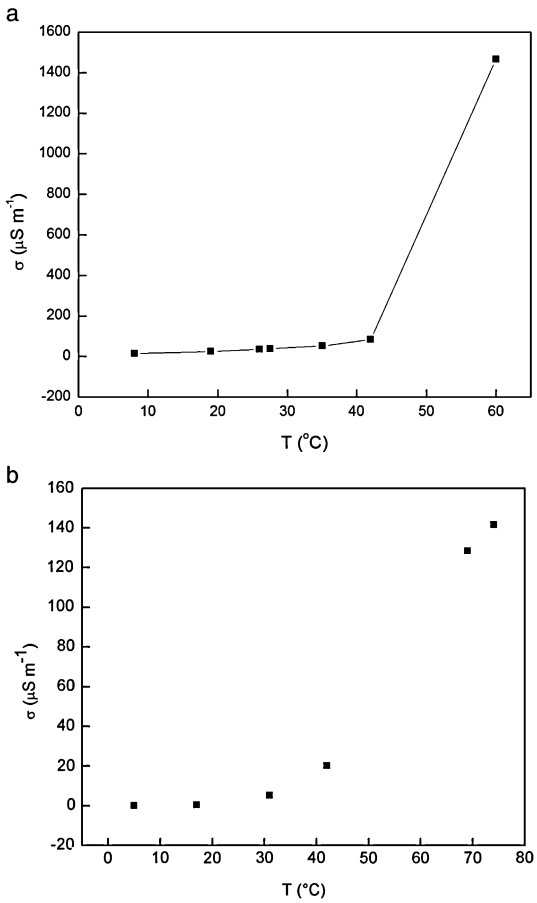

Fig. 4 Conductivities of (a) IL $[PhC_3MIm][NTf_2]$ **2b** and (b) IL $[C_2O_2MIm][Cl]$ **3** at different temperatures.

Nyquist plots. This strongly suggested that a charge transfer process of molecular oxygen at the platinum electrode surface was responsible for the observed phenomena, which is represented by the equilibrium reaction of Scheme 1.

This was further supported by the Nyquist plots obtained when the experiments were performed under a pure argon atmosphere and a pure oxygen atmosphere (Fig. S2, ESI†). The charge transfer process was not observed under an argon atmosphere. However, this process did take place in the presence of a pure molecular oxygen atmosphere.

The polarization resistance (R_P) values were determined by fitting the obtained impedance semicircles. The R_p values represent the polarization resistances related to the charge transfer process of oxygen on the platinum electrode surface, since the platinum electrode is inactive under the applied conditions. For all ILs **1–3**, R_P decreased with increasing temperatures. Eqn (1) was used to convert R_P into the conductivity (σ) of oxygen within the ILs, where l (0.1 cm) and A (3.14×10^{-2} cm^2) represent the length and active surface area of the working platinum electrode, respectively. These conductivities were due to charge transfer processes and transport phenomena of molecular oxygen and were not related to the ionic conductivities of the bulk ILs. This strategy was applied to determine the activation energies of the oxygen

$$O_{2,ads} \rightleftharpoons O_{2,ads}^{-}$$

Scheme 1 Charge transfer processes of molecular oxygen at the platinum electrode surface.

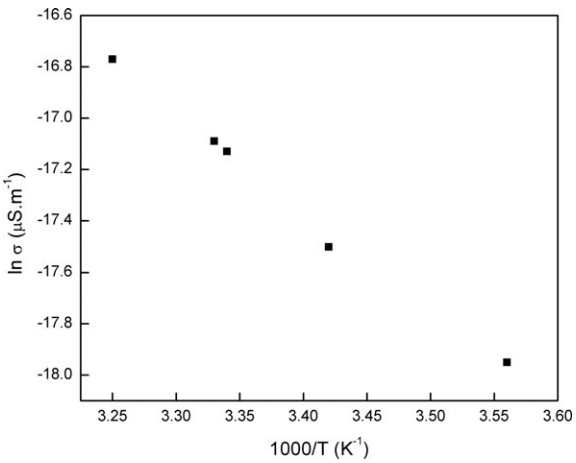

Fig. 5 Arrhenius conductivity plot of IL $[PhC_3MIm][NTf_2]$ **2b**.

Table 1 Activation energy, conductivity intersection and melting point of the ILs **1–3**

Entry	IL	E_a[a]/kJ mol^{-1}	E_a[a]/eV	T_{is}[b]/°C	T_m[c]/°C
1	[C_4MIm][Mes] **1a**	78.1	0.81	63	77
2	[C_{10}MIm][Mes] **1b**	79.0	0.82	31	57
3	[Ph_2C_2MIm][NTf_2] **2a**	73.7	0.76	40	62
4	[PhC_3MIm][NTf_2] **2b**	51.6	0.53	42	50
5	[PhC_2MIm][NTf_2] **2c**	56.6	0.58	28	41
6	[C_2O_2MIm][Cl] **3**	110	1.14	42	197 (204)[d]

[a] Activation energy calculated from the Arrhenius formula. [b] Temperature at the intersection of the low- and high-temperature range of the temperature dependent conductivity. [c] Melting point determined by differential scanning calorimetry on heating. [d] Ref. 42.

redox processes on the platinum electrode surface as described below.

$$\sigma = l/R_P A \quad (1)$$

Fig. 4(a) and (b) show the conductivities of the ILs [PhC_3MIm][NTf_2] **2b** and [C_2O_2MIm][Cl] **3** at different temperatures. The same conductivity–temperature correlation was observed for all ILs **1–3**. Higher temperatures resulted in higher conductivities. As such, the transport of the species involved in the charge transfer reaction is temperature dependent. Furthermore, the conductivity was characterized by two distinct temperature dependences: (1) small conductivity increases in the lower temperature range; and (2) large conductivity increases in the higher temperature range. In case of the ILs **2b** and **3**, these dependences showed their intersection at 42 and 35 °C, respectively, which indicates that the transport processes are differently affected below and above this temperature.

It was found that the experimental conductivity data of the lower temperature range fitted the conventional Arrhenius eqn (2), where E_a is the activation energy for the charge transfer process. Fig. 5 shows the Arrhenius conductivity plot of IL **2b** and the activation energies calculated from the Arrhenius formula are presented in Table 1. The hydrophilic ILs showed the higher charge transfer activation energies, which decreased in the order: [C_2O_2MIm][Cl] **3** > [C_{10}MIm][Mes] **1b** > [C_4MIm][Mes] **1a** > [Ph_2C_2MIm][NTf_2] **2a** > [PhC_2MIm][NTf_2] **2c** > [PhC_3MIm][NTf_2] **2b**. Now, it is important to remember that these activation energies were measured in the presence of atmospheric oxygen. The values of 51.6 kJ mol^{-1} (0.53 eV) to 110 kJ mol^{-1} (1.14 eV) are very close to those observed for charge transfer processes of oxygen at polycrystalline oxide surfaces,[46] LSCF-SDC composite[47] and multi-metallic electrodes.[48] Apparently, the determined IL charge transfer processes are due to electrochemical reactions of molecular oxygen at the electrode surface.[49]

$$\ln \sigma = \ln \sigma_0 - (E_a/RT) \quad (2)$$

3.2 X-Ray diffraction studies

The charge transfer processes involving molecular oxygen should be the same for all ILs **1–3**. As a consequence, it is reasonable to infer that the IL crystalline structure influences the transport of molecular oxygen inside the crystal. The crystal data concerning the ILs **2a–c** are listed in Table S5 (ESI†) and their structures at room temperatures are presented in Fig. 6. The electrostatic interactions of IL **2a** generate a tri-dimensional structural organization (Fig. 6(a)). In contrast, the existing interactions in the ILs **2b** and **2c** are of two-dimensional nature, generating structures in the form of layers as can be verified in Fig. 6(b) and (c). This structural organization at room temperature is reflected by the density of these ILs at room temperature, which decreases in the order: [PhC_3MIm][NTf_2] **2b** (d = 1.553 g cm^{-3}) > [PhC_2MIm][NTf_2] **2c** (d = 1.539 g cm^{-3}) > [Ph_2C_2MIm][NTf_2] **2a** (d = 1.47 g cm^{-3}). This suggests that a higher degree of two-dimensional organization as in IL **2b** results in a more dense packing. However, the observed activation energies decrease in exactly the opposite order: [Ph_2C_2MIm][NTf_2] **2a** > [PhC_2MIm][NTf_2] **2c** > [PhC_3MIm][NTf_2] **2b**. As a consequence, it is possible to infer that the diffusion of molecular oxygen is faster in two-dimensional organized ILs. Importantly, it is not possible to verify the formation of structures in the form of channels or tunnels.

3.3 Differential scanning calorimetry

The melting points of the ionic liquids **1–3** were determined by differential scanning calorimetry (DSC) to check if there exists a correlation with their temperature dependent conductivities (Table 1). Most of these ionic liquids have melting points that are close to their intersection temperatures as determined from the conductivity plots (*e.g.* Fig. 4). This indicates that the change from the slowly to the faster changing conductivity is most likely due to the changeover from the solid to the liquid state. In strong contrast, IL [C_2O_2MIm][Cl] **3** showed an intersection temperature (42 °C, Fig. 4(b)) far below its melting point (197 °C). As a consequence, IL **3** was not melted at the beginning of the second temperature range. This behavior allows us to infer that the faster increasing conductivity in the second temperature range of IL **3** should be associated with the oxygen diffusion inside the crystal arrays. A possible explanation could be an increase in fluxional behavior/reorientation phenomena in the solid state, which enhances the molecular oxygen diffusion.[50,51] This was further supported by the low degree of organization of IL **2c** observed at 25 °C by X-ray diffraction, and high quality data were only obtained at 100 K due to a more defined organization.

4. Conclusions

In conclusion, electrical impedance spectroscopy is a suitable analytical tool for the determination of important imidazolium IL properties, including polarization resistance (R_p), conductivity (σ) and activation energy (E_a) for a charge transfer reaction involving molecular oxygen. Increased temperatures result in higher conductivities, showing two distinct temperature ranges. The detected conductivities were due to charge transfer processes of molecular oxygen at the platinum electrode surface and mass transfer processes of oxygen inside the IL matrix. Comparison of the oxygen charge transfer process activation energies with the X-ray diffraction data of **2a–c** suggests that the oxygen mobility in the ionic liquids (solids at room temperature) is affected by their nature of structural supramolecular organization: tri-dimensional

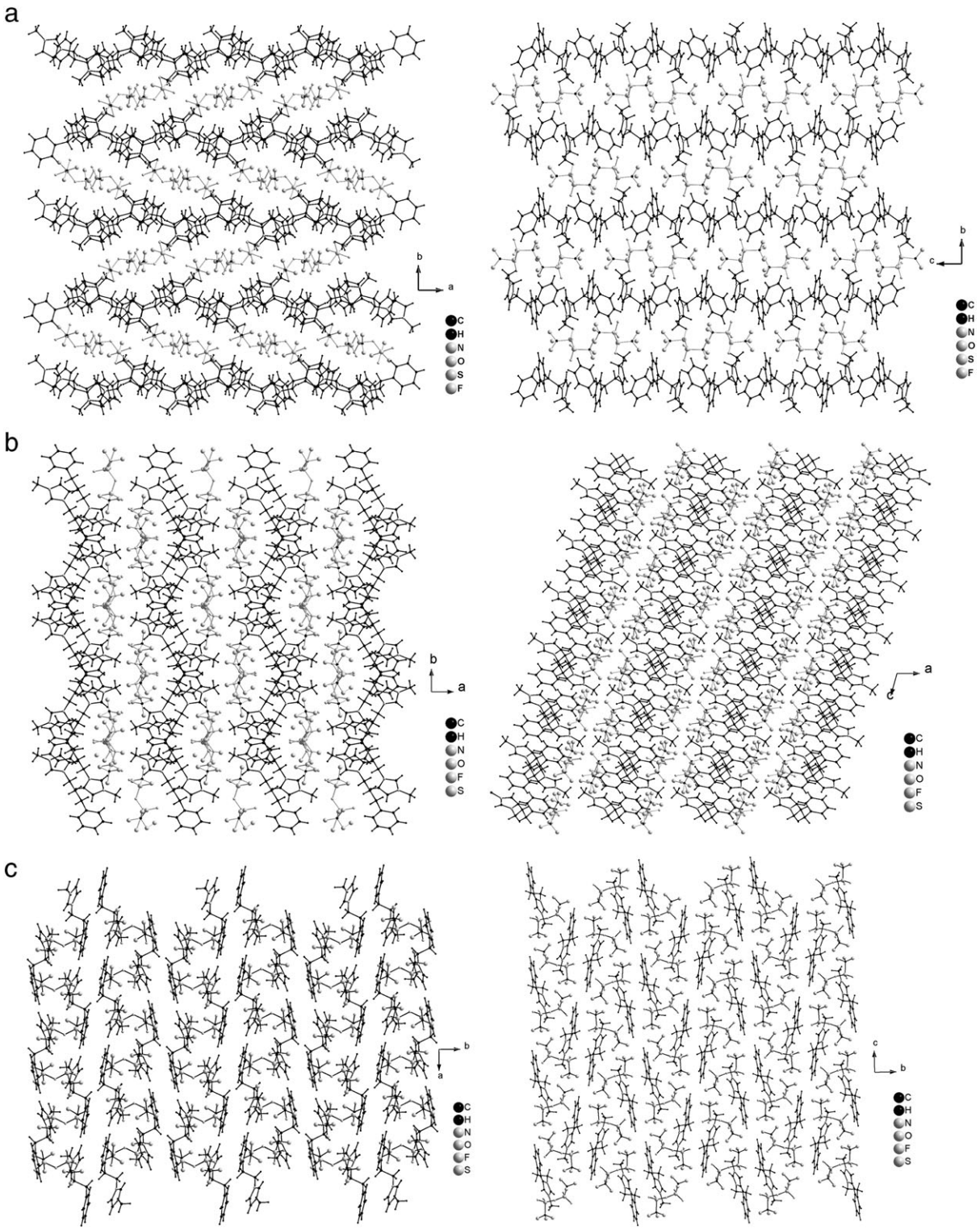

Fig. 6 X-Ray diffraction crystal structures of (a) $[Ph_2C_2MIm][NTf_2]$ **2a** (room temperature); (b) $[PhC_3MIm][NTf_2]$ **2b** (room temperature) and (c) $[PhC_2MIm][NTf_2]$ **2c** (100 K).

vs. two-dimensional. Furthermore, the changeover from the solid to the liquid state and fluxional behavior/reorientation phenomena in the solid state are most likely the responsible factors for the faster increasing conductivity in the second temperature range. As such, electrical impedance spectroscopy could accelerate the discovery of new electrochemical ionic liquid (solid at room temperature) applications and the substitution of ionic liquids where beneficial.

Acknowledgements

The authors thank the CNPq for financial support.

References

1 P. A. Z. Suarez, J. E. L. Dullius, S. Einloft, R. F. de Souza and J. Dupont, *Polyhedron*, 1996, **15**, 1217–1219.
2 F. Endres, D. MacFarlane and A. Abbott, *Electrodeposition from Ionic Liquids*, Wiley-VCH, Weinheim, Germany, 1st edn, 2008.
3 P. Wasserscheid and T. Welton, *Ionic Liquids in Synthesis*, Wiley-VCH, Weinheim, Germany, 1st edn, 2002, ch. 3–4, pp. 127–171.
4 J. Dupont, C. S. Consorti and J. Spencer, *J. Braz. Chem. Soc.*, 2000, **11**, 337–344.
5 J. Dupont, R. F. de Souza and P. A. Z. Suarez, *Chem. Rev.*, 2002, **102**, 3667–3692.
6 T. Welton, *Chem. Rev.*, 1999, **99**, 2071–2084.
7 H. S. Schrekker, M. P. Stracke, C. M. L. Schrekker and J. Dupont, *Ind. Eng. Chem. Res.*, 2007, **46**, 7389–7392.
8 S. G. Lee, *Chem. Commun.*, 2006, **10**, 1049–1063.
9 J. H. Davis, *Chem. Lett.*, 2004, **33**, 1072–1077.
10 Z. F. Fei, T. J. Geldbach, D. B. Zhao and P. J. Dyson, *Chem.–Eur. J.*, 2006, **12**, 2122–2130.
11 H. S. Schrekker, M. A. Gelesky, M. P. Stracke, C. M. L. Schrekker, G. Machado, S. R. Teixeira, J. C. Rubim and J. Dupont, *J. Colloid Interface Sci.*, 2007, **316**, 189–195.
12 J. G. Huddleston, H. D. Willauer, R. P. Swatloski, A. E. Visser and R. D. Rogers, *Chem. Commun.*, 1998, 1765–1766.
13 M. H. Abraham, A. M. Zissimos, J. G. Huddleston, H. D. Willauer, R. D. Rogers and W. E. Acree, Jr, *Ind. Eng. Chem. Res.*, 2003, **42**, 413–418.
14 T. Welton, *Coord. Chem. Rev.*, 2004, **248**, 2459–2477.
15 V. I. Pârvulescu and C. Hardacre, *Chem. Rev.*, 2007, **107**, 2615–2665.
16 D. Astruc, F. Lu and J. R. Aranzaes, *Angew. Chem., Int. Ed.*, 2005, **44**, 7852–7872; D. Astruc, F. Lu and J. R. Aranzaes, *Angew. Chem.*, 2005, **117**, 8062–8083.
17 P. Migowski and J. Dupont, *Chem.–Eur. J.*, 2007, **13**, 32–39.
18 A. Roucoux, J. Schulz and H. Patin, *Chem. Rev.*, 2002, **102**, 3757–3778.
19 L. S. Ott and R. G. Finke, *Coord. Chem. Rev.*, 2007, **251**, 1075–1100.
20 Z. Yang and W. Pan, *Enzyme Microb. Technol.*, 2005, **37**, 19–28.
21 M. A. Klingshirn, S. K. Spear, J. D. Holbrey and R. D. Rogers, *J. Mater. Chem.*, 2005, **15**, 5174–5180.
22 P. A. Z. Suarez, V. M. Selbach, J. E. L. Dullius, S. Einloft, C. M. S. Piatnicki, D. S. Azambuja, R. F. de Souza and J. Dupont, *Electrochim. Acta*, 1997, **42**, 2533–2535.
23 R. K. Donato, M. V. Migliorini, M. A. Benvegnú, J. Dupont, R. S. Gonçalves and H. S. Schrekker, *J. Solid State Electrochem.*, 2007, **11**, 1481–1487.
24 M. V. Migliorini, R. K. Donato, M. A. Benvegnú, J. Dupont, R. S. Gonçalves and H. S. Schrekker, *Catal. Commun.*, 2008, **9**, 971–975.
25 R. F. de Souza, J. C. Padilha, R. S. Gonçalves and J. Dupont, *Electrochem. Commun.*, 2003, **5**, 728–731.
26 S. Z. E. Abedin and F. Endres, *Chem. Phys. Chem.*, 2006, **7**, 58–61.
27 A. Lewandowski and A. Świderska, *Appl. Phys. A*, 2006, **82**, 579–584.
28 Q. Zhu, Y. Song, X. Zhu and X. Wang, *J. Electroanal. Chem.*, 2007, **601**, 229–236.
29 A. B. McEwen, H. L. Ngo, K. LeCompte and J. L. Goldman, *J. Electrochem. Soc.*, 1999, **146**, 1687–1695.
30 E. Stathatos, P. Lianos, V. Jovanovski and B. Orel, *J. Photochem. Photobiol., A*, 2005, **169**, 57–61.
31 N. Papageorgiou, Y. Athanassov, M. Armand, P. Bonhôte, H. Pettersson, A. Azam and M. Grätzel, *J. Electrochem. Soc.*, 1996, **143**, 3099–3108.
32 E. Markevich, V. Baranchugov and D. Aurbach, *Electrochem. Commun.*, 2006, **8**, 1331–1334.
33 R. F. de Souza, J. C. Padilha, R. S. Gonçalves, M. O. de Souza and J. Rault-Berthelot, *J. Power Sources*, 2007, **164**, 792–798.
34 F. Yang, L. Jiao, Y. Shen, X. Xu, Y. Zhang and L. Niu, *J. Electroanal. Chem.*, 2007, **608**, 78–83.
35 N. Matsumi, K. Sugai, M. Miyake and H. Ohno, *Macromolecules*, 2006, **39**, 6924–6927.
36 M.-A. Néouze, J. L. Bideau, P. Gaveau, S. Bellayer and A. Vioux, *Chem. Mater.*, 2006, **18**, 3931–3936.
37 F. Endres and S. Z. E. Abedin, *Phys. Chem. Chem. Phys.*, 2006, **8**, 2101–2116.
38 J. Dupont and P. A. Z. Suarez, *Phys. Chem. Chem. Phys.*, 2006, **8**, 2441–2452.
39 C. C. Cassol, G. Ebeling, B. Ferrera and J. Dupont, *Adv. Synth. Catal.*, 2006, **348**, 243–248.
40 H. S. Schrekker, D. O. Silva, M. A. Gelesky, M. P. Stracke, C. M. L. Schrekker, R. S. Gonçalves and J. Dupont, *J. Braz. Chem. Soc.*, 2008, **9**, 426–433.
41 M. P. Stracke, G. Ebeling, R. Cataluña and J. Dupont, *Energy Fuels*, 2007, **21**, 1695–1698.
42 S. V. Dzyuba and R. A. Bartsch, *ChemPhysChem*, 2002, **3**, 161–166.
43 J. K. Lee and M. J. Kim, *J. Org. Chem.*, 2002, **67**, 6845–6847.
44 M. E. Moret, A. B. Chaplin, A. K. Lawrence, R. Scopelliti and P. J. Dyson, *Organometallics*, 2005, **24**, 4039–4048.
45 Z. Fei, D. Zhao, T. J. Geldbach, R. Scopelitti and P. J. Dyson, *Chem.–Eur. J.*, 2004, **10**, 4886–4893.
46 H. Liu, C. Mojica-Calderon, S. B. Lyon and M. M. Stack, *Solid State Ionics*, 1999, **126**, 363–372.
47 C. Fu, K. Sun, N. Zhang, X. Chen and D. Zhou, *Electrochim. Acta*, 2007, **52**, 4589–4594.
48 P. S. Zhang, W. Zhang, F. Gerlach, K. Alborn and U. Guth, *Sens. Actuators B: Chem.*, 2005, **108**, 797–802.
49 A. Hetznecker, H. Kohler and U. Guth, *Sens. Actuators B: Chem.*, 2007, **120**, 378–385.
50 K. Pogorzelec-Glaser, J. Garbarczyk, C. Z. Pawlacczyk and E. Markiewicz, *Mater. Sci. Pol.*, 2006, **24**, 245–252.
51 G. R. Goward, K. Saalwächter, I. Fischbach and H. W. Spiess, *Solid State Nucl. Magn. Reson.*, 2003, **24**, 150–162.